

Composition dependent band gap and band edge bowing in AlInN: A combined theoretical and experimental study

S. Schulz,^{1,*} M. A. Caro,^{1,2} L.-T. Tan,^{3,†} P. J. Parbrook,^{1,4} R. W. Martin,³ and E. P. O'Reilly^{1,2}

¹Tyndall National Institute, Lee Maltings, Cork, Ireland

²Department of Physics, University College Cork, Ireland

³Department of Physics, SUPA, University of Strathclyde, Glasgow, United Kingdom

⁴School of Engineering, University College Cork, Ireland

(Dated: October 24, 2013)

A combined experimental and theoretical study is presented of the band gap of AlInN, confirming the breakdown of the virtual crystal approximation (VCA) for the conduction and valence band edges. Composition dependent bowing parameters for these quantities are extracted. Additionally, composition dependent band offsets for GaN/AlInN systems are provided. We show that local strain and built-in fields affect the band edges significantly, leading to optical polarization switching at much lower In composition than expected from a VCA approach.

PACS numbers: 71.15.Ap, 71.20.Nr, 71.22.+i, 78.55.Cr, 78.66.Fd

The semiconductor alloy $\text{Al}_{1-x}\text{In}_x\text{N}$ has a direct band gap that spans a very wide energy range (0.69 eV to 6.25 eV).¹ This basic property makes $\text{Al}_{1-x}\text{In}_x\text{N}$ an ideal candidate for a range of optoelectronic devices, such as laser diodes, light emitting devices and detectors.² To design $\text{Al}_{1-x}\text{In}_x\text{N}$ based devices, an accurate knowledge of the variation of the band gap E_g^{AlInN} with varying InN content x is required. Often the variation of the band gap of a semiconductor alloy with composition x can be successfully described by the so-called virtual crystal approximation (VCA)³

$$E_g^{\text{AlInN}} = (1-x)E_g^{\text{AlN}} + xE_g^{\text{InN}} - \tilde{b} \cdot x \cdot (1-x), \quad (1)$$

with a composition *independent* bowing parameter \tilde{b} .

However, for $\text{Al}_{1-x}\text{In}_x\text{N}$ systems a large range of values for the bowing parameter \tilde{b} have been reported in the literature. Reported values scatter from 2.5 eV, extracted from measurements on high x samples, up to 10 eV based on measurements with low x values.^{4,5} Hence, the assumption that \tilde{b} is independent of composition has been questioned by several groups.^{6,7} Recently, based on density functional theory (DFT) results, the physical mechanisms underlying this breakdown have been clarified. It has been shown that cation-related localized states in the conduction band (CB) and the valence band (VB) lead to the breakdown of the VCA.⁸ These results support the assumption of a composition *dependent* bowing parameter. It is important to note that when designing polarization matched GaN quantum wells (QWs), using AlInN barriers,^{9,10} the evolution of the CB edge (CBE) and VB edge (VBE) energies with InN content x is important, since this determines confinement energies for carriers.

To shed further light on the behavior of the band gap bowing in $\text{Al}_{1-x}\text{In}_x\text{N}$ and how CBE and VBE behave with varying InN content x , we have performed experimental and theoretical studies. Our results are compared with recent experimental literature data. We apply a tight-binding (TB) model, to achieve an atomistic

description of the electronic structure.¹¹ This model includes local strain and built-in fields arising from random alloy fluctuations in AlInN. The same approach has been successfully applied to InGaN alloys recently.¹¹

Our results confirm that the band gap bowing parameter in $\text{Al}_{1-x}\text{In}_x\text{N}$ is highly composition dependent and cannot be described by a simple VCA, Eq. (1). Furthermore, our calculations reveal that both CBE and VBE separately deviate from the VCA. Therefore, we also provide composition dependent bowing parameters for CBE and VBE in $\text{Al}_{1-x}\text{In}_x\text{N}$, which can then be used as input parameters for continuum-based descriptions, such as $\mathbf{k} \cdot \mathbf{p}$ -models, of AlInN heterostructures. Additionally, our theoretical analysis indicates that local strain and built-in fields, arising from random alloy fluctuations, play an important role in the description of the band edges, contributing therefore to the deviation from the VCA. We extract composition dependent CB and VB offsets for GaN/ $\text{Al}_{1-x}\text{In}_x\text{N}$ systems. Finally, we analyze the VB ordering in $\text{Al}_{1-x}\text{In}_x\text{N}$. We calculate an optical polarization switching from TM- to TE-polarized emission around $x = 0.15$.

On the experimental side, we have grown $\text{Al}_{1-x}\text{In}_x\text{N}$ epilayers with thicknesses about 100 nm by metal organic chemical vapor deposition, using GaN nucleation layers on *c*-plane sapphire. Here, $\text{Al}_{1-x}\text{In}_x\text{N}$ samples with x ranging from 0.082 to 0.17 have been studied by photoluminescence excitation (PLE) spectroscopy. The PLE measurements have been performed at low temperatures in a closed cycle helium cryostat. The samples have been excited by a Xe-lamp and the detected wavelength has been set to the $\text{Al}_{1-x}\text{In}_x\text{N}$ emission peak for each of the series of samples. The PLE spectra were fitted using a sigmoidal function, as introduced for InGaN epilayers in Ref. 12, to define the band gap energy together with a broadening of the absorption edge.

On the theoretical side, band gap and band edge bowing parameters have been studied by means of an *sp*³ TB model. This approach allows for a microscopic description of electronic and optical properties of AlInN. Our TB

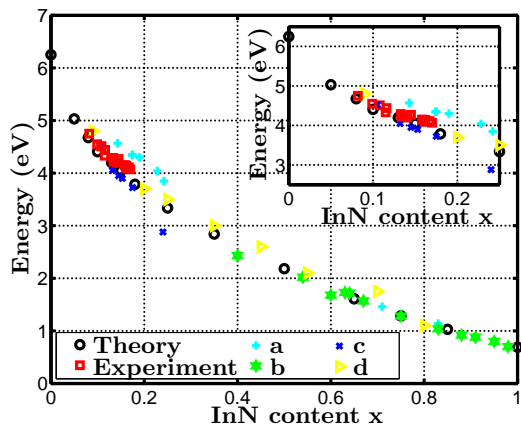
TABLE I: $\text{Al}_{1-x}\text{In}_x\text{N}$ composition dependent bowing parameters for band gap $[b]$, CB $[b^{\text{CB}}]$, and VB $[b^{\text{VB}}]$, as a function of x .

x	0.05	0.08	0.10	0.13	0.15	0.18	0.25	0.35	0.50	0.65	0.75	0.85
b (eV)	19.81	15.35	13.89	11.74	10.72	9.91	8.12	6.43	5.15	4.52	4.24	3.87
b^{CB} (eV)	14.01	10.67	9.29	7.67	7.01	6.23	4.95	3.92	3.08	2.54	2.22	1.96
b^{VB} (eV)	-5.80	-4.68	-4.59	-4.07	-3.71	-3.68	-3.17	-2.51	-2.07	-1.98	-2.01	-1.92

model includes explicitly local strain and built-in fields, arising from random alloy fluctuations. The theoretical framework is discussed in detail in Ref. 11 for InGaN systems. For AlInN we used the same approach; the required material parameters are taken from Refs. 10,13,14 while the AlN TB parameters can be found here.¹⁵

To gain insight into the behavior of the AlInN band gap and band edges, we have performed TB calculations on supercells containing approximately 12,000 atoms. The supercell is free to relax in all three spatial directions. For each InN content x , calculations for five different random configurations have been performed. The band gaps and band edges, at each composition, have been calculated as configurational averages. Details are given in Ref. 11.

Figure 1 shows our theoretical TB [black circles] and experimental PLE data [red squares] together with literature data. Overall, we find that our TB results are in very good agreement with the experimental data over the full composition range. Note that the TB approach involves fitting to the band gaps of the binary materials only. Also a closer look at the composition range $x = 0.05 - 0.25$, cf. inset Fig. 1, shows that both our theoretical and experimental results are in good agreement with the literature data. Furthermore, with as little as 5% InN [$x = 0.05$] in $\text{Al}_{1-x}\text{In}_x\text{N}$, a reduction in the band gap of over 1 eV is observed. This strong reduction in band gap can be traced back to In-related localized states



a: Ref. 7; b: Ref. 16; c: Ref. 5; d: Ref. 17

FIG. 1: Band gap of $\text{Al}_{1-x}\text{In}_x\text{N}$ as a function of x . Our theoretical [open circles] and experimental results [squares] are compared to literature data.

in the CB.⁸ As discussed in Ref. 8, these localized states lead to the breakdown of the simple VCA description. Consequently, a composition dependent bowing parameter is required, labeled b in the following.

Table I summarizes the calculated values for b in $\text{Al}_{1-x}\text{In}_x\text{N}$ as a function of x , obtained from our TB model. This data is derived using Eq. (1) by fitting to the end points (binaries) and the desired x -value. Especially in the low InN regime extremely large values for b are observed.

However, when modeling AlInN-based heterostructures, not only the overall band gap bowing is important but also how the band gap bowing is distributed between CB and VB. This quantity is of central importance for an accurate description of electronic and optical properties of heterostructures since it determines the confinement energies for the carriers.

Figure 2 shows the TB results for the CBE [circles] and VBE [squares] in $\text{Al}_{1-x}\text{In}_x\text{N}$ as a function of x . A VCA fit to the TB data over the whole composition range is given by the dashed-(dotted) lines and is obtained from

$$\begin{aligned} E_{\text{CB}}^{\text{AlInN}} &= x(E_g^{\text{InN}} + \Delta E_{\text{VB}}) + (1-x)E_g^{\text{AlN}} - \tilde{b}^{\text{CB}}x(1-x), \\ E_{\text{VB}}^{\text{AlInN}} &= x\Delta E_{\text{VB}} - \tilde{b}^{\text{VB}}x(1-x). \end{aligned} \quad (2)$$

Here, \tilde{b}^{CB} and \tilde{b}^{VB} are composition *independent* and the VB offset ΔE_{VB} between InN and AlN is taken from Ref. 18. Figure 2 confirms again that composition *independent* bowing parameters fail to describe the CBE and VBE in AlInN. The behavior of the CBE can clearly

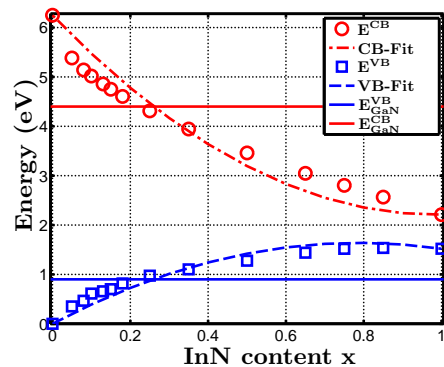
FIG. 2: CBE and VBE in $\text{Al}_{1-x}\text{In}_x\text{N}$ as a function of x . TB results for CBE and VBE [E^{CB} ; E^{VB}]: open symbols; dashed-(dotted) lines: fit obtained from Eq. (2). Solid horizontal lines: GaN CBE and VBE, respectively.

TABLE II: VB and CB offset $\Delta E_{\text{VB}}^{\text{GaN}/\text{AlInN}}$ and $\Delta E_{\text{CB}}^{\text{GaN}/\text{AlInN}}$, respectively, between GaN and $\text{Al}_{1-x}\text{In}_x\text{N}$ as a function of x .

x	0	0.05	0.08	0.10	0.13	0.15	0.18	0.25	0.35	0.50	0.65	0.75	0.85	1
$\Delta E_{\text{CB}}^{\text{GaN}/\text{AlInN}}$ (eV)	1.85	0.98	0.74	0.62	0.46	0.35	0.20	-0.09	-0.46	-0.94	-1.35	-1.60	-1.83	-2.19
$\Delta E_{\text{VB}}^{\text{GaN}/\text{AlInN}}$ (eV)	0.90	0.55	0.43	0.29	0.24	0.20	0.08	-0.07	-0.20	-0.38	-0.54	-0.62	-0.64	-0.62

not be described by the VCA [dashed-dotted line]. The VBE shows a similar behavior, but with a smaller deviation from a VCA-like model. To a first approximation a composition *independent* VB bowing parameter could be used [$\tilde{b}^{\text{VB}} = -2.64$ eV].

We apply the procedure described above for the composition dependent band gap bowing parameter b to CBE and VBE. The values for CBE and VBE bowing parameters b^{CB} and b^{VB} , respectively, are summarized in Table I. From Table I we conclude that the very strong composition dependence of the AlInN band gap in the low InN regime mainly arises from the composition dependence of the CBE. In this regime the CBE bowing parameter b^{CB} is much larger than the VBE parameter b^{VB} . This finding ties in with recent DFT results on the low InN regime.⁸ However, since we observe also a significant VBE bowing parameter, the commonly applied assumption¹⁹ in which all the bowing is attributed to the CB seems to fail in AlInN, especially when studying higher InN contents ($x > 0.5$), since b^{CB} and b^{VB} are comparable in magnitude for that range.

Having discussed the composition dependence of both the band gap and band edges in $\text{Al}_{1-x}\text{In}_x\text{N}$, we turn now and focus on the effect that local alloy, strain and built-in field fluctuations have on the results. In Fig. 3 we disentangle the impact of these quantities on CBE [Fig. 3 (a)] and VBE [Fig. 3 (b)]. We start with the analysis of the CBE. Comparing the results in the absence of the local strain and built-in potential contributions [$E_{\epsilon=0, \phi=0}^{\text{CB}}$; open stars] with data when including local strain effects only [$E_{\epsilon \neq 0, \phi=0}^{\text{CB}}$; open squares] we observe a strong shift of the CBE to higher energies. This shift to higher energies arises from the deformation potential correction due to local hydrostatic strain, since the interatomic bond lengths of InN are larger ($\approx 14\%$) than those of AlN. When also including the local built-in potential fluctuations [$E_{\epsilon \neq 0, \phi \neq 0}^{\text{CB}}$; open circles], we observe almost no difference between this full calculation and the situation where we have switched off the built-in potential fluctuations [$E_{\epsilon \neq 0, \phi=0}^{\text{CB}}$; open squares], at least on the energy scale shown.

Figure 3 (b) shows the situation for the VBE. Taking local strain effects into account but neglecting local built-in potential contributions [$E_{\epsilon \neq 0, \phi=0}^{\text{VB}}$; open squares], one observes a shift of the VBE to higher energies compared to the situation when only local alloy effects [$E_{\epsilon=0, \phi=0}^{\text{VB}}$; open stars] are included. The effect is mainly related to local compressive strains. In the presence of the local built-in field contributions [$E_{\epsilon \neq 0, \phi \neq 0}^{\text{VB}}$; circles], we observe a further upward bowing of the VBE compared to the

situation without the local built-in potential [$E_{\epsilon \neq 0, \phi=0}^{\text{VB}}$; open squares]. These results are similar to our findings on the band edges in $\text{In}_x\text{Ga}_{1-x}\text{N}$.¹¹

Having discussed how band edges change in $\text{Al}_{1-x}\text{In}_x\text{N}$ with x , we estimate in the following the composition dependent CB and VB offsets $\Delta E_{\text{CB}}^{\text{GaN}/\text{AlInN}}$ and $\Delta E_{\text{VB}}^{\text{GaN}/\text{AlInN}}$, respectively, between GaN and AlInN. Here, we estimate band offsets in the absence of strain and polarization fields. When band offsets are included, for example, in QW calculations by means of $\mathbf{k} \cdot \mathbf{p}$ -theory, strain and built-in potentials will be added separately.²⁰ Here, the VB offset $\Delta E_{\text{VB}}^{\text{GaN}/\text{AlInN}}$ is calculated as $\Delta E_{\text{VB}}^{\text{GaN}/\text{AlInN}} = \Delta E_{\text{VB}}^{\text{GaN}/\text{AlN}} - E_{\text{VB}}^{\text{AlInN}}$, where $E_{\text{VB}}^{\text{AlInN}}$ is obtained from Eqs. (2) using data from Table I. $\Delta E_{\text{VB}}^{\text{GaN}/\text{AlN}}$ denotes the VB offset between GaN and AlN. We assume $\Delta E_{\text{VB}}^{\text{GaN}/\text{AlN}} = 0.9$ eV, which is in the range of reported literature values [$\Delta E_{\text{VB}}^{\text{GaN}/\text{AlN}} = 0.15 - 1.4$ eV],²¹⁻²⁴ and at $x = 1$, $|E_{\text{VB}}^{\text{GaN}/\text{InN}}| = 0.62$ eV in accordance with Ref. 24 for the VB offset between InN and GaN. Our approach is similar to the approach used in Ref. 19. Therefore, if $\Delta E_{\text{VB}}^{\text{GaN}/\text{AlInN}} > 0$ the VBE in GaN is at higher energies than the VBE in AlInN. The composition dependent CB offset, $\Delta E_{\text{CB}}^{\text{GaN}/\text{AlInN}}$, is calculated as $\Delta E_{\text{CB}}^{\text{GaN}/\text{AlInN}} = E_{\text{CB}}^{\text{AlInN}} - (\Delta E_{\text{VB}}^{\text{GaN}/\text{AlN}} + E_g^{\text{GaN}})$, where

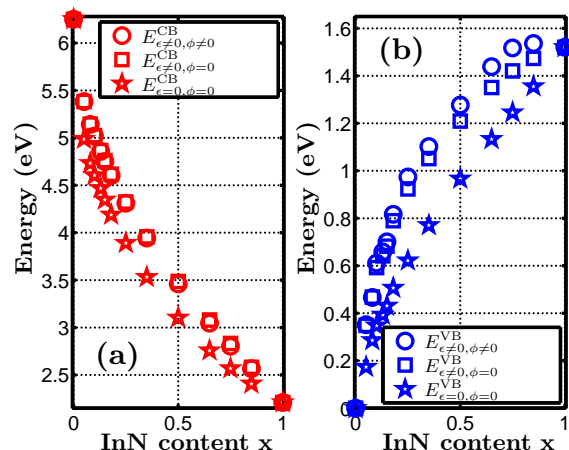


FIG. 3: CBE (a) and VBE (b) of $\text{Al}_{1-x}\text{In}_x\text{N}$ as a function of x . Open stars: Without strain and built-in potential ($E_{\epsilon=0, \phi=0}^{\text{VB/CB}}$); Open squares: With strain but without built-in potential ($E_{\epsilon \neq 0, \phi=0}^{\text{VB/CB}}$); Open circles: With strain and built-in potential ($E_{\epsilon \neq 0, \phi \neq 0}^{\text{VB/CB}}$).

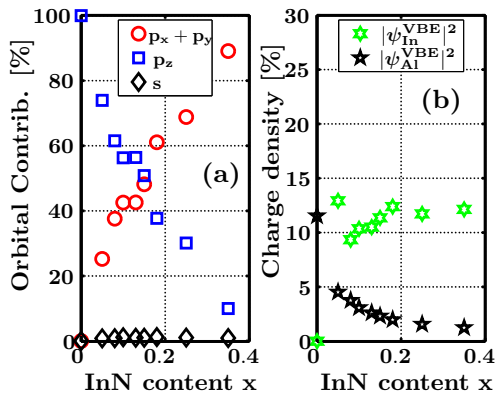


FIG. 4: (a) Orbital contributions to the VBE. (b) Charge density at In- and Al-atoms for the VBE. The data is shown as a function of x in $\text{Al}_{1-x}\text{In}_x\text{N}$.

E_g^{GaN} is the bulk band gap of GaN.¹ $E_{\text{CB}}^{\text{AlInN}}$ is calculated from Eqs. (2) using data from Table I. Here, $\Delta E_{\text{CB}}^{\text{GaN/AlInN}} > 0$ indicates that the CBE in GaN is at lower energies than the CBE in AlInN.

The obtained results are summarized in Table II where we estimate that the VB and CB offsets are positive up to 25% InN in AlInN. In terms of a heterostructure, neglecting strain and built-in potentials, this indicates that electrons and hole are confined in the GaN region. For $x \geq 0.25$ we observe a change in sign in CB and VB offsets, indicating that the carriers are confined in the AlInN region. We note that there is an uncertainty in the calculated composition values where CB and VB offset change sign due to the uncertainty in the AlN/GaN VB offset;^{21–24} an increase (decrease) in the assumed VB offset would for instance lead to the CB crossover occurring at lower (higher) InN compositions.

In the final step we study how the optical polarization due to the VB ordering changes in $\text{Al}_{1-x}\text{In}_x\text{N}$ with x . Compared to more conventional III-V semiconductors such as InAs, the spin-orbit coupling (SOC) in the group-III nitrides is small.^{25,26} Neglecting the weak SOC, the topmost VB in AlN is p_z -like while in InN it is a linear combination of p_x - and p_y -like states. Figure 4 (a) shows the contribution of the s -, p_x -, p_y - and p_z -like orbitals to

the VBE in fully relaxed $\text{Al}_{1-x}\text{In}_x\text{N}$ as a function of x . Our TB results show that below $x = 0.15$, the dominant orbital contribution is still p_z -like, while for $x > 0.15$ the linear combination of p_x - and p_y -like states starts to dominate. Therefore, our data indicates an optical polarization switching [TM to TE] in $\text{Al}_{1-x}\text{In}_x\text{N}$ at $x = 0.15$. Performing calculations for AlInN systems pseudomorphically grown on GaN, the polarization switching occurs at $x \approx 0.18$ (not shown). Figure 4 (b) illustrates that the charge density on the In-sites ($|\psi_{\text{In}}^{\text{VBE}}|^2$) increases significantly compared to the Al-sites ($|\psi_{\text{Al}}^{\text{VBE}}|^2$) with as little as 5% InN in the system (remainder of the charge density is on the N-sites). This indicates a strong localization of the wave function around the In sites, in agreement with recent DFT data,⁸ and explains the surprisingly early onset of the polarization switching.

In summary we have studied the band gap bowing of AlInN as a function of the InN content x both experimentally and theoretically. Our atomistic TB results are in good agreement with the performed PLE measurements and with experimental literature data. We confirm that the assumption of a composition *independent* bowing parameter fails and provide data for the composition dependence of the bowing parameter. Moreover, we find that both CBE and VBE show deviations from a simple VCA description. Composition dependent VBE and CBE bowing parameters have been extracted.

Our microscopic analysis reveals that local strain and built-in field effects play a significant role in the composition dependent behavior of CBE and VBE. We have used this data to study the band offsets in AlInN/GaN systems. Our analysis of the optical polarization in AlInN shows a switching from TM- to TE-polarized emission at 15 – 18% InN.

This work was supported by Science Foundation Ireland (project No. 10/IN.1/I2994, 10/IN.1/I2993 and 07/EN/E001A), the Engineering and Physical Sciences Research Council and the European Union Project ALIGHT (FP7-280587). We are grateful to the crystal growth teams at Strathclyde University, Cambridge University and CRHEA-CNRS, Valbonne who provided the AlInN samples measured for this work.

* Electronic address: stefan.schulz@tyndall.ie

† Present address: School of Engineering, Republic Polytechnic, 9 Woodlands Ave 9, Singapore 738964

¹ J. Wu: J. Appl. Phys. **106**, 011101 (2009).

² G. Liu, J. Zhang, X.-H. Li, G. S. Huang, T. Paskova, K. R. Evans, H. Zhao, and N. Tansu: J. Cryst. Growth **340**, 66 (2012).

³ L. Nordheim: Ann. Phys. (Leipzig) **9**, 607 (1931).

⁴ K. S. Kim, A. Saxler, P. Kung, M. Razeghi, and K. Y. Lim: Appl. Phys. Lett. **71**, 800 (1997).

⁵ T. Aschenbrenner, H. Dartsch, C. Kruse, M. Anastasescu, M. Stoica, M. Gartner, A. Pretorius, A. Rosenauer, T.

Wagner, and D. Hommel: J. Appl. Phys. **108**, 063533 (2010).

⁶ K. Wang, R. W. Martin, D. Amabile, P. R. Edwards, S. Hernandez, E. Nogales, K. P. O'Donnell, K. Lorenz, E. Alves, V. Matias, A. Vantomme, D. Wolverson, and I. M. Watson: J. Appl. Phys. **103**, 073510 (2008).

⁷ E. Sakalauskas, H. Behmenburg, C. Hums, P. Schley, G. Rossbach, C. Giesen, M. Heuken, H. Kalisch, R. H. Jansen, J. Bläsing, A. Dadgar, A. Krost, and R. Goldhahn: J. Phys. D: Appl. Phys. **43**, 365102 (2010).

⁸ S. Schulz, M. A. Caro, and E. P. O'Reilly: arXiv:1307.5985 [cond-mat.mtrl-sci] (2013).

- ⁹ M. A. Caro, S. Schulz, S. B. Healy, and E. P. O'Reilly: *J. Appl. Phys.* **109**, 084110 (2011).
- ¹⁰ M. A. Caro, S. Schulz, and E. P. O'Reilly: *Phys. Rev. B* **86**, 014117 (2012).
- ¹¹ M. A. Caro, S. Schulz, and E. P. O'Reilly: arXiv:1309.3309 [cond-mat.mtrl-sci] (2013).
- ¹² R. W. Martin, P. G. Middleton, K. P. O'Donnell, and W. Van der Stricht: *Appl. Phys. Lett.* **74**, 263 (1999).
- ¹³ A. D. Andreev and E. P. O'Reilly: *Phys. Rev. B* **62**, 15851 (2000).
- ¹⁴ Q. Yan, P. Rinke, M. Winkelkemper, A. Qteish, D. Bimberg, M. Scheffler, and C. G. Van de Walle: *Semicond. Sci. Technol.* **26**, 014037 (2011).
- ¹⁵ TB parameters for AlN: $E(s, a) = -10.20$ eV, $E(p, a) = 0.66$ eV, $E(p_z, a) = 0.92$ eV, $E(s, c) = 2.25$ eV, $E(p, c) = 11.08$ eV, $V(s, s) = -8.11$ eV, $V(x, x) = 3.20$ eV, $V(x, y) = 5.63$ eV, $V(sa, pc) = 3.04$ eV, $V(pa, sc) = 10.31$ eV
- ¹⁶ R. E. Jones, R. Broesler, K. M. Yu, J. W. Ager, E. E. Haller, W. Walukiewicz, X. Chen, and W. J. Schaff: *J. Appl. Phys.* **104**, 123501 (2008).
- ¹⁷ E. Iliopoulos, A. Adikimenakis, C. Giesen, M. Heuken, and A. Georgakilas: *Appl. Phys. Lett.* **92**, 191907 (2008).
- ¹⁸ P. D. C. King, T. D. Veal, P. H. Jefferson, C. F. McConville, T. Wang, P. J. Parbrook, H. Lu, and W. J. Schaff: *Appl. Phys. Lett.* **90**, 132105 (2007).
- ¹⁹ O. Ambacher, J. Majewski, C. Miskys, A. Link, M. Hermann, M. Eickhoff, M. Stutzmann, F. Bernardini, V. Fiorentini, V. Tilak, B. Schaff, and L. F. Eastman: *J. Phys.: Condens. Matter* **14**, 3399 (2002).
- ²⁰ L. C. Lew Yan Voon and M. Willatzen, *The $\mathbf{k} \cdot \mathbf{p}$ Method: Electronic Properties of Semiconductors* (Springer, Heidelberg, 2009).
- ²¹ G. Martin, A. Botchkarev, A. Rockett, and H. Morkoc: *Appl. Phys. Lett.* **68**, 2541 (1996).
- ²² W. Mönch: *J. Appl. Phys.* **80**, 5076 (1996).
- ²³ N. Binggeli, P. Ferrara, and A. Baldereschi: *Phys. Rev. B* **63**, 245306 (2001).
- ²⁴ P. G. Moses, M. Miao, Q. Yan, and C. G. Van de Walle: *J. Chem. Phys.* **134**, 084703 (2011).
- ²⁵ I. Vurgaftman, J. R. Meyer, and L. R. Ram-Mohan: *J. Appl. Phys.* **89**, 5815 (2001).
- ²⁶ I. Vurgaftman and J. R. Meyer: *J. Appl. Phys.* **94**, 3675 (2003).